POAC'15
Trondheim, Norway

Proceedings of the 23rd International Conference on
Port and Ocean Engineering under Arctic Conditions
June 14-18, 2015
Trondheim, Norway

NUMERICAL APPROACH OF TIME DOMAIN SIMULATION FOR ICE BREAKING SHIP IN LEVEL ICE

Donghyeong Ko, Kyoungsoo Ahn, Kyungduk Park

Hyundai Heavy Industries Co., Ltd.

ABSTRACT

Ice breaking process and patterns in level ice of ice breaking ship are numerically calculated in time domain. For commercial ice breaking ships, ice resistance increases excessively in ice breaking procedure with constant crushing stress. Thus, varying crushing stress depending on the velocity vectors and the contact area is newly introduced to reproduce its breaking patterns around the ships in detail. It is assumed that ice resistance is comprised of three parts: breaking, buoyancy and clearing parts. In this paper, the breaking part is mainly focused on because it is critical to numerical resistance evaluation for ice breaking ship design. To verify the numerical calculation, the assessed ice resistances are compared with ice model test results. The buoyancy and clearing parts are obtained from the empirical formula of Lindqvist(1989). Additionally, this scheme is applied to turning simulation.

1. INTRODUCTION

For ice breaking ship design, it is necessary to evaluate ice resistance and load to confirm whether the ship satisfies the specific requirements such as, minimum ice breaking speeds and turning ability in a certain ice condition and given power.

For the evaluation of ice resistance, several empirical formulas were introduced by Shimanskii(1938), Enkvist(1972) and Lindqvist (1989) which uses the basic hull information such as length, breadth, depth, hull angles and etc. The formulas give a certain level of accuracy but they cannot predict the breaking pattern considering the breaking pattern precisely. Similarly, empirical formula by Park et al. (2014) which takes the design load water line and the under-water hull form into account, improved the prediction of speed performance, but it also has the same problems.

Biao Su. (2011) suggested the time-domain numerical simulation based on ice breaking procedure with constant crushing stress. This method well represents the ice breaking patterns and the turning ability, and it shows good agreement with full scale measurements for an ice breaker by Riska et al. (2001). However, the commercial ice breaking ships in this paper has long parallel middle body, so the ice resistance increased dramatically in time domain simulation in case of the constant crushing stress. So, in this paper, varying crushing stress was applied to avoid the problem. The varying crushing stress is related with linear velocity vector, angular velocity vector and contact area between ship and ice fragments.

2. NUMERICAL SIMULATION

2.1. Modeling for ice resistance estimation

Basic formulation is the same as the thesis of Biao Su.(2011). Ice resistance is comprised of three parts: breaking, buoyancy and clearing parts. In this paper, the breaking part is mainly focused on, and the buoyancy and clearing parts are obtained from the empirical formula of Lindqvist(1989). The numerical simulation process is denoted by a flow chart in Figure 1.

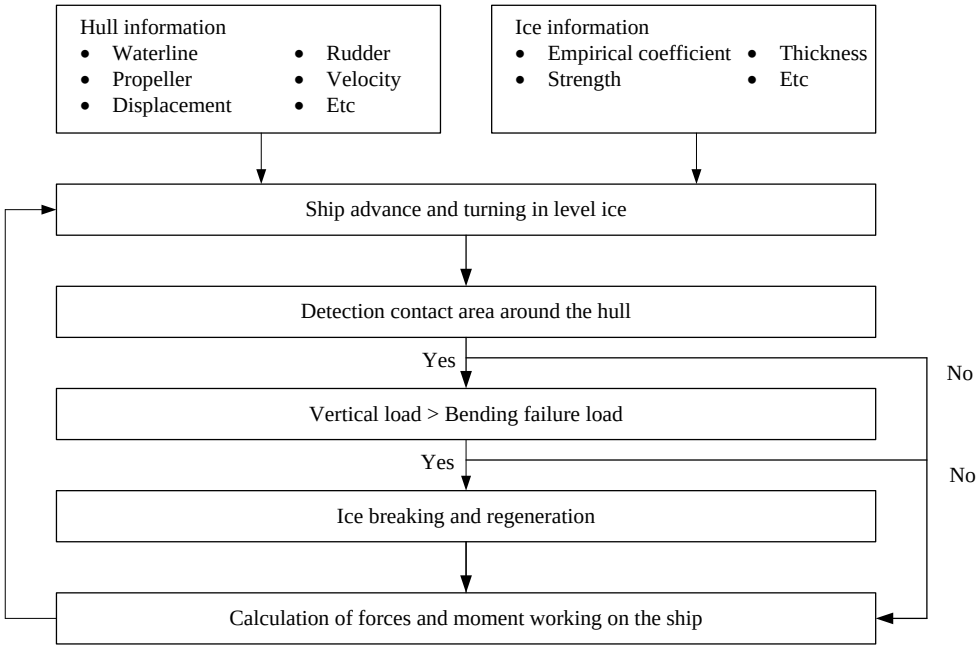

Figure 1 Flow chart of numerical simulation

Initial inputs are hull and ice information such as waterline shape of hull, propeller open water characteristics and ice properties. Ice is marked in discretized nodes. As ship moves on, the code calculates the contact area around the hull and checks whether its vertical load exceeds the bending failure load. If the bending failure occurs, the ice geometry is regenerated and then forces and moment working on the ship is calculated. During the process, as shown in Figure 2, unconnected nodes with ship are excluded to enhance the computational efficiency.

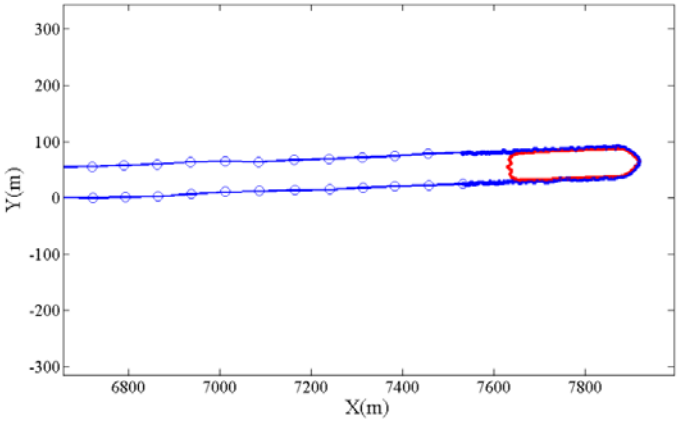

Figure 2 Description of node generation (ice nodes is highlighted by circles).

Biao Su (2011) proposed the constant crushing stress to calculate ice load in level ice, but it was found that the ice load dramatically increased around the ship in case of long parallel middle body.

To solve this problem, concept of varying crushing stress with respect to velocity vectors and contact area is introduced. According to Ashby et al. (1986), the relationship between crushing stress and size of contact area is explained in equation (1) and Figure 3.

$$\sigma_{area} = \frac{P}{A} = \frac{p_L \Delta_L}{L_i^3}\left[1+3\left(\frac{L_i^3}{A\Delta_L}\right)^{\frac{1}{2}}\right] \tag{1}$$

where, L_i is dimension of cubical independent cells, Δ_L is a moved distance before the cell fails and p_L is the average force during the period of contact.

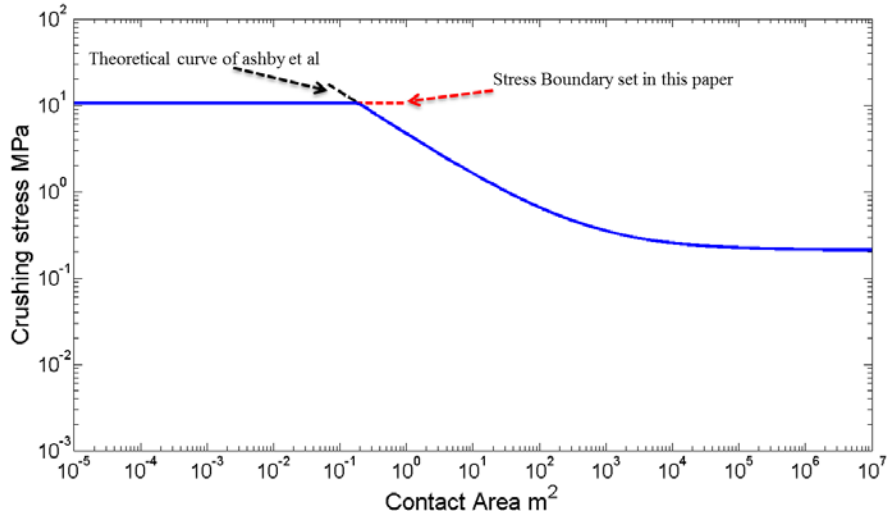

Figure 3 Theoretical curve of Ashby et al. (1986) bounded by the collected data

In figure 3, the crushing stress soars infinitely as contact area decreases to zero. Thus, in this paper, the maximum stress was limited to 10.5MPa referring to the experimental data of Sanderson (2014).

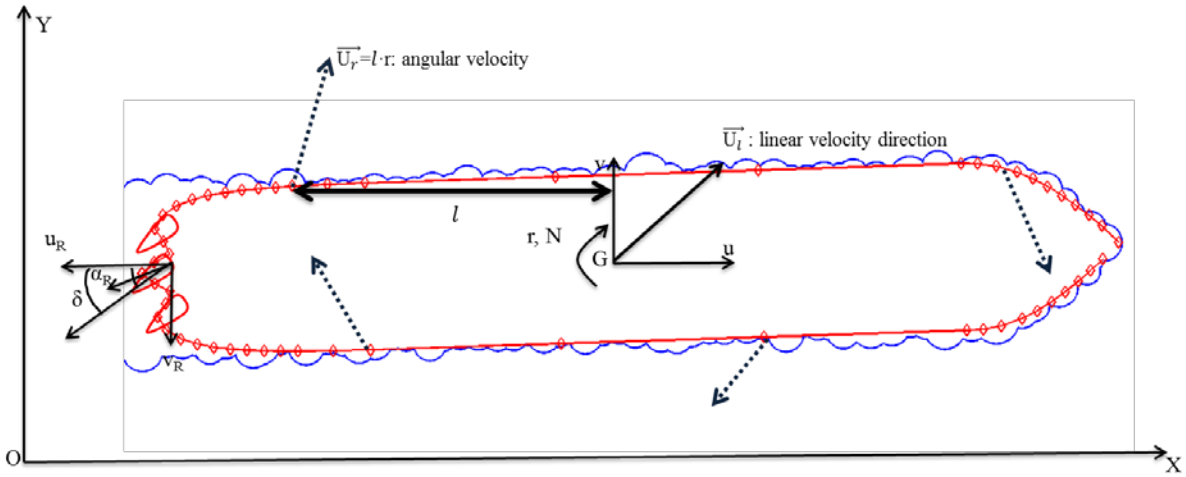

Figure 4 Schematic diagram of coordinate systems

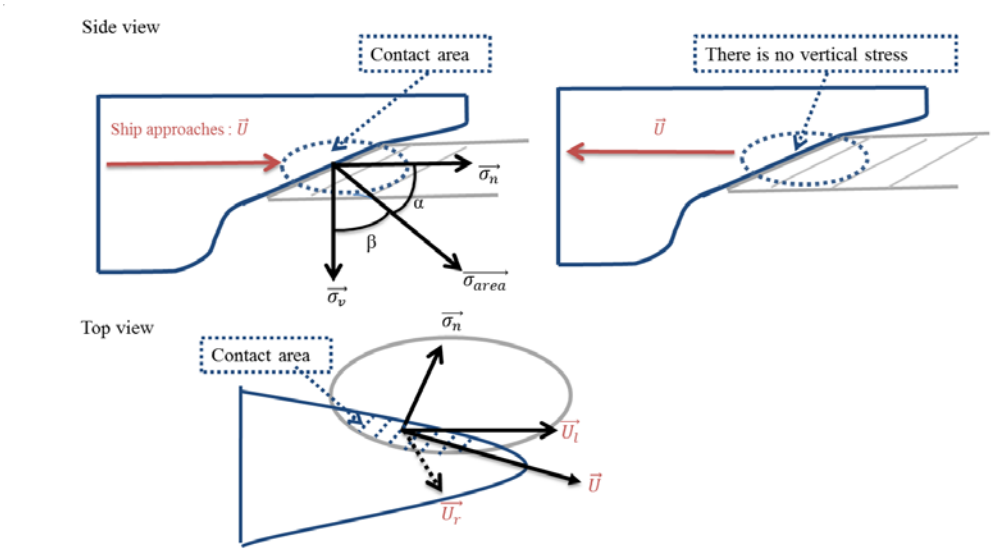

Figure 5 Description of contact area and crushing stress

In crushing stress calculation, ship advance direction is considered as well as the size of contact area. In figure 4, waterline of the ship is represented by nodes. All nodes have equivalent linear velocity. However, angular velocity and slope angle between ship and ice fragment (α, β) are different in every position, but easily obtained from those of the proximate node. Working direction of crushing stress is composed two velocity vectors: linear velocity ($\overrightarrow{U_l}$) and angular velocity ($\overrightarrow{U_r}$). Thus, crushing stress align with total velocity vector ($\vec{U}$) which is the summation of two velocity vectors.

$$\vec{U} = \overrightarrow{U_l} + \overrightarrow{U_r} \tag{2}$$

As shown in figure 5, vertical stress (σ_v) and crushing stress (σ_n) act only if ship approaches ice fragment. Vertical stress in the side view is the cosine β component of σ_{area} and crushing stress in the top view is computed by inner product between velocity vector and inward normal vector of ice fragment. Crushing stress is not to exceed σ_{area} and its minimum is set to zero. These are summarized in the equation (3) and (4).

$$\begin{aligned} \sigma_n &: \sigma_{area} \cdot t_1 \cdot \cos\alpha \\ \sigma_v &: \sigma_{area} \cdot t_2 \cdot \cos\beta \end{aligned} \tag{3}$$

$$t_1 : \begin{cases} \dfrac{\vec{U} \cdot \overrightarrow{\sigma_n}}{|\vec{U}| \cdot |\overrightarrow{\sigma_n}|} : & if \ \dfrac{\vec{U} \cdot \overrightarrow{\sigma_n}}{|\vec{U}| \cdot |\overrightarrow{\sigma_n}|} > 0 \\ 0 : & else \end{cases},$$

$$t_2 : \begin{cases} 1 : & if \ \dfrac{\vec{U} \cdot \overrightarrow{\sigma_n}}{|\vec{U}| \cdot |\overrightarrow{\sigma_n}|} > 0 \\ 0 : & else \end{cases}, \tag{4}$$

Where, $\overrightarrow{\sigma_n}$ is the crushing stress vector in inward normal direction of ice fragment, $\overrightarrow{U_l}$ is the linear velocity component and $\overrightarrow{U_r}$ is the angular velocity component.

As a result, the ice resistance and its ship speed with time developed are denoted in Figure 6 and 7. In the figures, dotted lines show ice resistance with suggested crushing stress in this paper which considered ship advance direction and size of contact area. However, solid lines represent varying stress with ship advance direction only (figure 6) and constant crushing stress (figure 7).

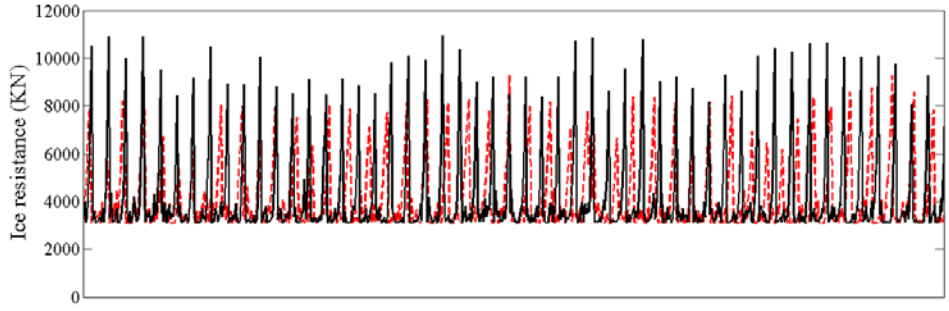

Figure 6 Ice resistance difference between suggested crushing stress and varying stress with ship advance direction only.

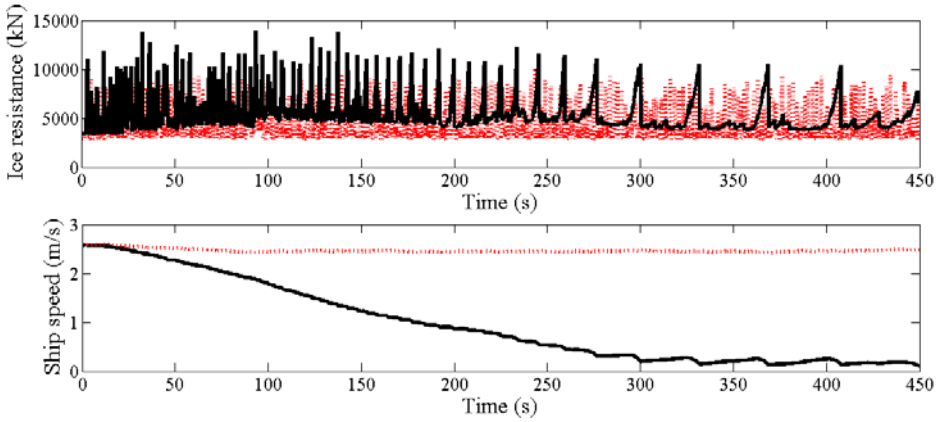

Figure 7 Comparison of ice load and ship speed between suggested crushing stress and constant crushing stress.

2.2. Simulation of ship performance based on modular model

Modular type mathematical model was used to analyze the turning ability. The coordinate system is in Figure 4. Because the ship has three azipod propulsors, three azipods are considered in the formulation. So, force and moments including ice load can be defined by equation (4).

$$\begin{aligned}(M+M_x)\cdot\dot{u} &= X_H + X_P + X_R + X_{ice} + (M+M_x)\cdot v\cdot r \\ (M+M_y)\cdot\dot{v} &= Y_H + Y_P + Y_R + Y_{ice} - (M+M_y)\cdot u\cdot r \\ (I_{zz}+J_{zz})\cdot\dot{r} &= N_H + N_P + N_R + N_{ice}\end{aligned} \tag{4}$$

Where,

M_x : added mass in surge motion

M_y : added mass in sway motion

J_{zz} : added moment in yaw motion

Hydrodynamic derivatives of hull

$$\begin{aligned}X_H &= X_{vr}vr + X_{vv}v^2 + X_{rr}r^2 \\ Y_H &= Y_v v + Y_r r + Y_{vvv}v^3 + Y_{rrr}r^3 + (Y_{vrr}r + Y_{rvv})vr \\ N_H &= N_v v + N_r r + N_{vvv}v^3 + N_{rrr}r^3 + (N_{vrr}r + N_{rvv})vr\end{aligned} \tag{5}$$

POD propeller

$$\begin{aligned}X_P &= (1-t)\left(T^P + T^C + T^S\right)\cos\delta \\ Y_P &= (1-t)\left(T^P + T^C + T^S\right)\sin\delta \\ N_P &= x_P(1-t)\left(T^P + T^C + T^S\right)\sin\delta - y_P(1-t)\left(T^P + T^C + T^S\right)\cos\delta\end{aligned} \tag{6}$$

Where,

x_P : x - directional position of POD

y_P : y - directional position of POD

$$T = \rho n^2 D_P^4 K_T(J_P, v_P)$$

$$u_P^{PC,S} = (1 - w_P^{P,C,S})u$$

$$w_P^{P,C,S} = w_{P0} \exp(-C_P^{P,C,S} v_P^2)$$

$$v_P = v + x_P r$$

POD strut

$$\begin{aligned} X_R &= (1 - t_R)\left(F_N^P + F_N^C + F_N^S\right)\sin\delta \\ Y_R &= (1 + a_H)\left(F_N^P + F_N^C + F_N^S\right)\cos\delta \\ N_R &= (x_R + a_H x_H)\left(F_N^P + F_N^C + F_N^S\right)\cos\delta - y_R(1 - t_R)\left(F_N^P - F_N^S\right)\sin\delta \end{aligned} \tag{7}$$

Where,

$$F_N^{P,C,S} = \frac{\rho}{2} A_R \left(U_R^{P,C,S}\right)^2 f_\alpha \sin\left(\alpha_R^{P,C,S}\right)$$

$$U_R^{P,C,S} = \sqrt{\left(u_R^{P,C,S}\right)^2 + \left(v_R^{P,C,S}\right)^2}$$

$$u_R^{P,C,S} = \varepsilon^{P,C,S} u_P^{P,C,S} \sqrt{\eta\left\{1 + \kappa^{P,C,S}\left(\sqrt{1 + \frac{8K_T}{\pi J^2}} - 1\right)\right\}^2 + (1 - \eta)}$$

$$u_P^{P,C,S} = (1 - w_P^{P,C,S})u$$

$$w_P^{P,C,S} = w_{p0} \exp(-C_P^{P,C,S} v_P^2)$$

$$v_R^{P,C,S} = -\gamma_R^{P,C,S}(v + l_R r)$$

$$\alpha_P^{P,C,S} = \delta - \delta_0^{P,C,S} + \frac{v_R^{P,C,S}}{u_R^{P,C,S}}$$

3. RESULTS

3.1 Speed performance

For three different ships, the numerical simulations for forward ice breaking performance were carried out and their results are compared with model test results. Among three ships, model tests of ship A and ship B are conducted at ice model basin A, and model test of ship B is carried out at ice model basin B. Table 1 shows the principal dimensions of the ships.

The numerical simulation runs 10,000 s computation times. The ice thickness is set to 1.5 m. Flexural strengths are 500 kPa for ship A and ship B (ice model basin A), 600 kPa for ship C (ice model basin B) respectively. Figure 8 shows the ice breaking patterns of ship A and ship C. the breaking patterns connected by ice nodes are recorded at each time step. Because ship C has larger bow angle and lower speed than ship A, the cusp on the center line of ship C is bigger than ship A.

Table 1 Principal dimensions of ships

	SHIP A	SHIP B	SHIP C
L/B	5.5	6.0	5.5
B/T	4.3	3.9	4.3
Bow angle	20 deg.	20 deg.	25 deg.

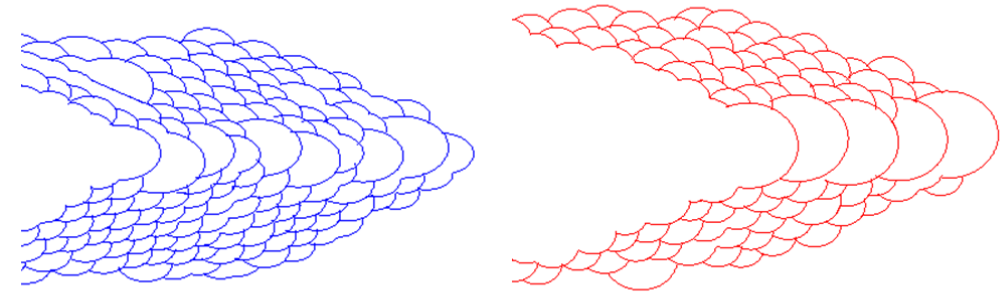

Figure 8 Breaking patterns of ship A(left) and ship C(right)

Three vessel's speeds at 100% MCR power are compared at Figure 9. The POD propellers used in model basin A was different from ones in model basin B. Although the net thrust (total propeller thrust minus the open water resistance at the same speed) and rps are not exactly same, in this paper, the POD propeller characteristics of model basin A were all applied in the numerical simulation for direct comparison. Average speed at 100% MCR power in the simulation is 2.4 m/s (ship A), 2.6 m/s (ship B) and 1.1 m/s (ship C). Model test results were 2.5 m/s (ship A), 2.7 m/s (ship B) and 1.3 m/s (ship C).

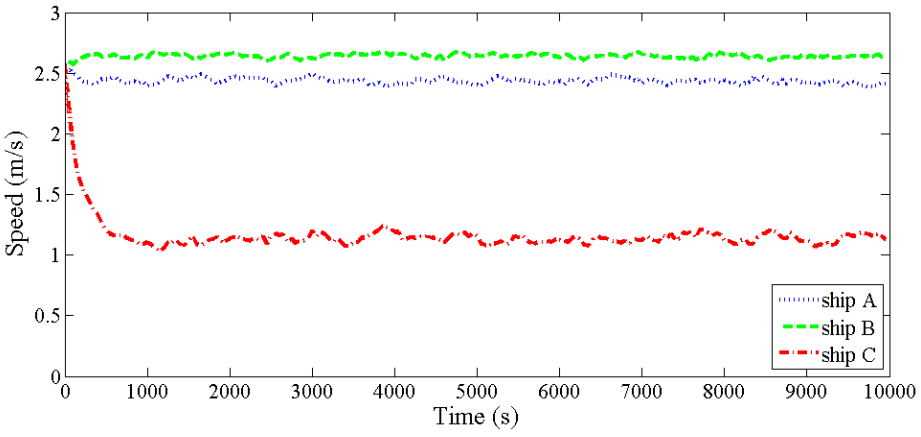

Figure 9 Time history of speeds at 100% MCR power

Speed-ice resistance relations between simulation and model test are compared and the results are presented in Figure 10. The ice resistance at 100% MCR power in the numerical simulation well corresponds to model test result, but the gradient is relatively lower than model test.

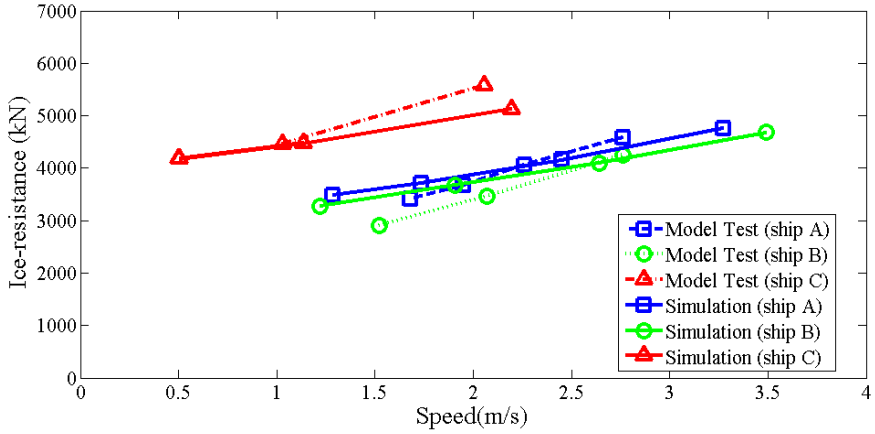

Figure 10 Comparative speed-ice resistance between simulation and model test.

3.2 Turning performance

Figure 11 shows the turning ability of all ships. Ice thickness and flexural strength are 1.5 m and 500 kPa for ship A and ship B(ice model basin A) and 1.53 m and 820 kPa for ship C(ice model basin B) respectively. The diameters of turning circle were obtained after 360 degree turn, but those of the model tests were extrapolated from initial turning path because of the limitation of tank size. Change of heading in initial path was from 3 to 9 degree.

Model test results are 9,300 m (ship A), 15,000 m (ship B) and 6,000 m (ship C). During the simulation, the ship was stuck in the ice due to the difference of resistance from model tests. Thus, to match up turning speed with model tests, 150% MCR power was applied to all numerical simulations. As a result, turning diameters from simulation are 9,500 m (ship A), 15,600 m (ship B) and 7,800 m (ship C) respectively.

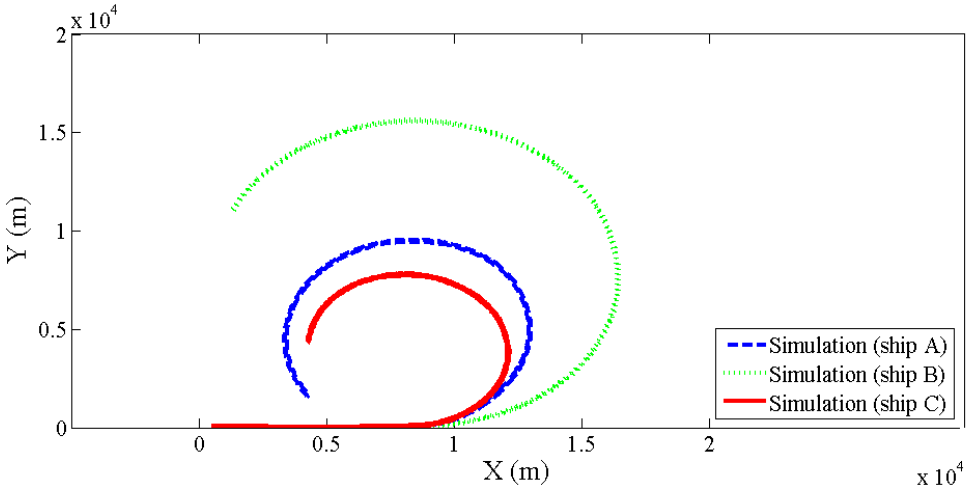

Figure 11 Turning ability simulations of three model ships.

4. CONCLUSION

Time domain simulation for ice breaking patterns and manouevrability was studied and it is compared with model test results. In this study, varying crushing stress with respect to contact area and velocity vector are suggested to solve the problem of excessive crushing stress around long parallel middle body in commercial ice breaking ships and to reflect ship's hull form variation. The crushing stress could be regulated by the above suggestion.

Above all, considering the relation between contact area and crushing stress, the theoretical curve of Ashby et al. (1986) was applied and the crushing stress was bounded by 10.5MPa referring to the experimental data. In addition, considering ship advance, the inner product of the ship's velocity vector and the normal vector of contact area was applied to the crushing stress.

Ice model test results were carried out to verify the ice resistance and turning ability. It well reflects the difference of hull form. In addition, speed and turning performance in level ice can be well predicted. However, the gradient of ice resistance according to the speed is relatively lower than model test results. Until now, ice breaking patterns, ice resistance and turning ability depending on ship design were focused on. In order to enhance the accuracy of crushing stress according to speed, more model test data should be needed.

5. REFERENCES

Ashby, M.F., Palmer,A.C., Thouless, M., Goodman, D.J., Howard, M.W., Hallam, S.D., Murrell, S.A.F., Jones, N., Sanderson, T.J.O. and Ponter, A.R.S, 1986. Nonsimultaneous failure and ice loads on Arctic structures. Offshore Technology Conference 1986 NO. OTC 5127, pp. 399-404, Houston, USA.

Enkvist, E., 1972. On the Ice Resistance Encountered by Ships Operating in the Continuous Mode of Icebreaking. Report No.24, The Swedish Academy of Engineering Science in Finlande, Helsinki, Finland.

Izumiyama, K., Wako, D., Shimoda, H. and Uto, S., 2005. Ice load measurement on a model ship hull. Proceedings of 18TH International Conference on Port and Ocean Engineering under Arctic Conditions (POAC), New York, USA.

Park, K.D. and Kim, H.S., 2014. Study on the Ship Ice Resistance Estimation Using Empirical Formulas. Proceedings of the ASME 2014 33rd International Conference on Ocean, Offshore and Arctic Engineering (OMAE), San Francisco, USA.

Lindqvist, G., 1989. A straightforward method for calclation of ice resistance of ships. Proceedings of 10th International Conference on Port and Ocean Engineering under Arctic Conditions (POAC), Lulea, Sweden.

Riska, K.,Leiviska, T., Nyman, T., Fransson, L.,Lehtonen, J., Eronen, H. and Backman,

A.,2001. Ice Performance of the Swedish Multi-Purpose Icebreaker Tor Viking Ⅱ. Proceedings of PAC 2001, pp.849-865.

Sanderson T.J.O, 2014, Ice Mechanics. Springer, Lexington, USA.

Schneider, P.J. and Eberly, D.H., 2002. Geometric Tools for Computer Graphics. Morgan Kaufmann Publishers, San Francisco, USA.

Shimanskii, Y.A., 1938. Conditional standards of ice qualities of a ship. Trans. Arctic Research Institute, Northern Sea Route Administration Publishing House, Vol. 130, Leningrad. Translation T-381-01 by Engineering Consulting and Translation Center (ECTC), P.O. Box 1377, Jackson Heights, New York, NY 11372.

Su, B, 2011. Numerical Predictions of Global and Local Ice Loads on Ships. PH.D. Thesis. Department of Marine Technology, Norwegian University of Science and Technology, Norway.

Yeon-gyu K., Sunyoung K., Youngha P., Byeongseok Y. and Sukwon L., Prediction of Maneuverability of a Ship with POD Propulsion System. Journal of the Society of Naval Architects of Korea Vol. 43, No. 2, pp. 164-170